ELSEVIER

Oceanologica Acta 25 (2002) 101–116

ACTA International Journal of Oceanology

www.elsevier.com/locate/oceat

Modelling subsurface dynamics in the Black Sea

Modélisation de la dynamique de sub-surface en Mer Noire

Gökay Karakaş *, Alec James, Alaa Al-Barakati

Environmental Technology Centre, UMIST, P.O. Box 88, Manchester M60 1QD, UK

Received 14 March 2001; received in revised form 5 December 2001; accepted 28 February 2002

Abstract

Dependency of major hydrophysical/chemical features of highly stratified basins on density surfaces in the vertical makes isopycnic models an attractive tool for simulating the dynamics of marginal marine environments such as the Black Sea because of the ability of these models to restrict vertical transport to some desirable degree. In the present work the seasonal variations of the subsurface dynamics of the Black Sea are investigated using an isopycnic model. Particular attention is given to the interfaces of the Cold intermediate layer and Suboxic layer and finally, the deep layer circulation in the basin is studied. It appears that although the depth range of the base of the Cold intermediate layer and the lower Soboxic layer interface do not change seasonally, their horizontal distribution is defined by the upper layer dynamics of the basin. Cyclonic surface circulation diminishes with increasing depth and the deep layer circulation is characterised by an anti-cyclonic rim current driven by density gradients created from river runoff and the influx of Mediterranean water. © 2002 Ifremer/CNRS/IRD/Éditions scientifiques et médicales Elsevier SAS. All rights reserved.

Résumé

La liaison entre les facteurs hydrologiques et chimiques et les densités de surface dans les mers stratifiées rend attractive l'utilisation de modèles isopycnaux pour simuler la dynamique de mers comme la mer Noire. Ce modèle réduit en effet le transport vertical à un niveau acceptable. Les variations saisonnières de la dynamique de sub-surface de la Mer Noire ont été simulées en se servant d'un modèle isopycne. Une attention particulière a été portée aux interfaces entre la couche intermédiaire froide et la couche faiblement oxygénée. Finalement, la circulation profonde du bassin est étudiée. Alors que le niveau d'immersion de la base intermédiaire et de l'interface inférieure de la couche sous- oxygénée ne présentent pas de fluctuations saisonnières, leur répartition horizontale dépend de la dynamique de la couche de surface. La circulation cyclonique superficielle diminue quand la profondeur augmente et la circulation profonde est caractérisée par un courant annulaire anticyclonique entraîné par le gradient de densité crée par l'apport d'eau douce et l'entrée d'eau méditerranéenne. © 2002 Ifremer/CNRS/IRD/Éditions scientifiques et médicales Elsevier SAS. Tous droits réservés.

Keywords: Black Sea; Isopycnic modelling; Cold intermediate layer; Sub-oxic layer; Deep rim counter-current

Mots clés: Mer noire; Modèle isopycne; Couche intermédiaire froide; Couche sous-oxygénée; Contre-courant profond

1. Introduction

In terms of physical characteristics, the Black Sea started to take its present form when its connection with the Mediterranean opened again about 7000 years ago. In the deep water layers the salinity increased as a result of the inflow of salt water from the Sea of Marmara while in the surface layers it decreased because of the inflow of fresh river water from melting glacial ice. As a consequence of these changes, strong density stratification occurred and anaerobic conditions were established in the bottom layers and the interface between the oxygenated upper waters and hydrogen sulphide rich deeper waters has risen to its present

* Corresponding author : UFZ, Centre for Environmental Research, Department of Inland Water Research, Brueckstr. 3a, 39114 Magdeburg, Germany.
E-mail address: karakas@gm.ufz.de (G. Karakaş).

PII: S0399-1784(02)01185-4

depth of about 150 m. This interfacial region, which is only a few tens of metres thick, is known as the Suboxic layer (SOL) and coincides with the permanent halocline (Sorokin, 1983; Ozsoy and Unluata, 1997).

The Cold intermediate layer (CIL), which is characterised by temperatures less than 8 °C, is another special feature of the Black Sea. This low temperature layer is usually located below the seasonal thermocline and can be seen throughout the basin. The CIL is preserved through the year by strong vertical gradients in the seasonal and permanent haloclines that prevent the water in the CIL from mixing with adjacent layers. A survey conducted in September 1991 (HydroBlack'91) revealed that the CIL extends down to ≈100 dbar, where the density anomaly, σ_t, reaches 15.65 kg m^{-3}. In contrast the density anomaly at its upper boundary is 14.15 kg m^{-3}. The average minimum temperature observed during the survey was ≈7.2 °C (σ_t ≈ 14.4–14.5 kg m^{-3}). The SOL lies below the CIL, and extends to a depth of 140 dbar, where σ_t = 16.2 kg m^{-3}. This corresponds to the base of the permanent pycnocline. The SOL is similar to the CIL regarding its thickness and confinement to shallower depths in the cyclonic regions (Oguz et al., 1994).

At this time, the mechanisms underlying the genesis of the CIL are not fully understood. Filippov (1965) and Tolmazin (1985) argue that it is formed in the northwestern shelf region and in the proximity of the Kerch Strait. In contrast Ovchinnikov and Popov (1987) suggest that the CIL waters are formed in the centres of cyclonic eddies. On the other hand, Ozsoy and Unluata (1997) argue that although available satellite and hydrographic observations suggest the formation of a cold and dense water mass in the northwestern shelf region, these data provide inadequate support for a direct relation between these waters and the CIL. In another study, Ivanov et al. (1997) analysed volumetrically the temperature and salinity of the cold intermediate water masses using the data sets obtained in recent years. These authors argue that for a cold winter Ovchinnikov and Popov's hypothesis is more realistic and contribution of northwestern shelf to the cold water production is relatively small. This observation is supported by the results of surveys made along the Turkish coast in September '88 and April '89 that show the CIL is deeper and thicker in the coastal areas than in the centre (Oguz et al., 1991).

The results of the September '88 and April '89 surveys also provide a means of investigating the seasonal variations in the CIL. In the results of the April '89 survey, the upper boundary of the CIL is found at about 25 m and the layer is relatively thick following the formation of new CIL-water during the winter. The lower boundary lies at about 100–150 m or further down in the anti-cyclonic eddies. The September '88 results, on the other hand, indicate a thinner CIL due to the decrease in the amount of newly formed CIL waters. Its upper boundary lies at about 40 m in the western and at 50 m in the eastern basin, while the lower boundary extends to relatively higher levels, about 100 m (Oguz et al., 1991).

The main features of the circulation in the upper layer of the Black Sea are a basin-wide cyclonic current system flowing along the continental slope, called the rim current (or the Main Black Sea current in the former Soviet literature), and a series of mesoscale eddies confined by the coast and the rim current. The eddies, sizes of which change from sub-basin scale gyres to sub-mesoscale features, are interconnected with each other by jets and filaments. The meandering rim current, being a basin-scale feature of the circulation, is characterised by either one elongated cell covering the whole basin, or by a series of separate cyclonic cells located in the western and eastern parts of the basin depending on the season and on the wind curl. It is reported that circulation is more intense and better organised in winter than in summer, that is, when the circulation is seasonally persistent, more eddy activity is observed in various scales (Titov, 1992; Eremeev et al., 1996; Ginsburg, 1995). The rim current can be thought to constitute a buffer zone between coastal and offshore waters and so is a very important feature of the circulation system in terms of the biogeochemistry of the basin. The driving mechanisms for the circulation are reported to comprise the curl of the wind stress distribution, the thermohaline fluxes and the topography although it is still not clearly understood which of these predominates. Recent studies and surveys show that the Black Sea has very strong temporal and mesoscale variabilities and a complex, interrelated and eddy dominated circulation.

The circulation in deep layers of the Black Sea is also subject to debate. Following the HydroBlack '91 survey, Oguz et al. (1994) suggest that even though the large scale components of the general circulation remain similar down to 500 dbar, both large and mesoscale features of the circulation are subject to considerable changes at increased depth. The SO'90 survey shows not only the disappearance of the rim current, the shift of eddy centres, the coalescence of eddies, and the persistence of some components but also structural changes in the deeper layers (Oguz et al., 1993). Bulgakov and Kushnir (1996), after carrying out investigations based on theoretical analysis and laboratory tests, conducted field observations and concluded that an anti-cyclonic counter current lies below the rim current at the depth of the main pycnocline in the northern and northwestern parts of the basin. Similarly, Eremeev and Kushnir (1996), based on the measurements conducted during ComsBlack surveys in August 1992 and in October-November 1993, point out that under certain conditions a counter current may be formed under the rim current in the same region. However, observations over the whole basin are lacking. Korotaev (1997) constructed a simple, non-linear model to investigate the circulation in a circular basin with a depth of 2000 m under the influence of lateral buoyancy fluxes, like river inflow and saline water input. His simulation predicts a three-layer structure of the circu

lation. A cyclonic circulation is developed in the upper 100 m. The anti-cyclonic undercurrent of intermediate depths extends down to 1800 m. In the very deep layer he reports a weak cyclonic current.

Recently, it has been demonstrated that various physical and chemical characteristics of the Black Sea (e.g. the oxic/anoxic transition layer, the so-called suboxic zone, the cold intermediate layer, the seasonal variations of phosphates, nitrates and dissolved oxygen, etc.) develop on density surfaces and show little variation over the basin (Murray et al., 1991; Saydam et al., 1993; Oguz et al., 1994; Ivanov et al., 1997). A number of scientists, therefore, started to examine the basin wide data in order to define the temporal and spatial variability in the density-dependent profiles of the major hydrochemical properties of the basin (see Tugrul et al. (1992), Basturk et al. (1997)).

To date, the study of the dynamics of the basin making use of numerical models has been limited to traditional depth and sigma coordinate models, which seem unable to produce realistic descriptions of stratification and deep layer circulation. Elsewhere it is claimed that a density-dependent definition of a range of physical and chemical processes is more informative for the study of long-term change in the vertical hydrophysics/chemistry of the Black Sea (Konovalov et al., 1997). Therefore the isopycnic approach, where the vertical coordinate system is related to potential density layers, provides a promising option for the more realistic simulation of these processes. To this end we have set up a circulation model of the Black Sea in isopycnic coordinates to extend our understanding of the vertical dynamics of the basin so to allow better description of biogeochemical processes. In this short contribution we restrict our efforts to the presentation of simulation results of subsurface layers dynamics, namely CIL and SOL interfaces and deep layer circulation.

2. Model description

Ocean general circulation models, until recently, have been usually developed using cartesian co-ordinates. However, when the conservation equations for salt and temperature are written in the *x,y* and *z* directions, it is difficult to avoid excessive diapycnal mixing in long term simulations. Theoretical consideration of the adiabatic character of fluid motion and eddy diffusion over long time scales has brought about a new type of model that reduces the truncation errors introduced when approximating finite-difference equations or numerical errors resulting from physically incorrect splitting of the transport and diffusion processes into their vertical and horizontal components. In contrast to conventional multi-level models for stratified fluids, isopycnic models comprise a set of constant potential density layers. Since oceanic mixing processes take place predominantly along constant potential density surfaces, these models where the dynamic equations are changed from (*x, y,* z) to (*x, y, ϱ)* coordinates achieve a more accurate representation of the physical system, provided that the resolution is sufficient. Here ϱ is the potential density. The reader is referred to Bleck (1978) for a complete description of the transformation of the governing equations from the cartesian to isopycnic form. The result of this change is that transport in the *x* and *y* directions occurs on isopycnic surfaces while transport in the *z* direction is now in the parallel to the ϱ axis. Transport in this direction can be totally suppressed so that the diapycnal component can be suppressed unless required. Accordingly, spurious heat exchange between warm surface waters and cold bottom waters are minimised as well as horizontal heat exchange along sloping isopycnal surafaces such as those in frontal regions (Chassignet et al., 1996).

2.1. Governing equations

The model used in the present study has three prognostic equations, namely the equations for mass conservation, the horizontal velocity vector and the conservation of buoyancy related variables such as density, salt and temperature. These are written respectively as:

$$\frac{\partial}{\partial t_s}\left(\frac{\partial p}{\partial s}\right) + \nabla_s \cdot \left(\vec{v}\,\frac{\partial p}{\partial s}\right) + \frac{\partial}{\partial s}\left(\dot{s}\,\frac{\partial p}{\partial s}\right) = 0 \qquad (1)$$

$$\frac{\partial \vec{v}}{\partial t_s} + \nabla_s \frac{\vec{v}^{\,2}}{2} + (\xi + f)\, k \times \vec{v} + \left(\dot{s}\,\frac{\partial p}{\partial s}\right)\frac{\partial \vec{v}}{\partial p} + \nabla_a M = -\, g\,\frac{\partial \tau}{\partial p} + \left(\frac{\partial p}{\partial s}\right)^{-1} \nabla_s \cdot \left(\nu\,\frac{\partial p}{\partial s}\nabla_s \vec{v}\right) \qquad (2)$$

$$\frac{\partial}{\partial s}\left(\frac{\partial p}{\partial s}T\right) + \nabla_s \cdot \left(\vec{v}\,\frac{\partial p}{\partial s}T\right) + \frac{\partial}{\partial s}\left(\dot{s}\,\frac{\partial p}{\partial s}T\right) = \nabla_s \cdot \left(\nu\,\frac{\partial p}{\partial s}\nabla_s T\right) + H_T \qquad (3)$$

where *s* is an arbitrary isopycnal surface in the vertical, $\vec{v} = (u,v)$ is the horizontal velocity vector, *p* is pressure, $\alpha = p^{-1}$ is the specific volume, $\xi = \partial v/\partial x_s - \partial u/\partial y_s$ is the relative vorticity, $m = gz + p\alpha$ is the Montgomery potential, *gz* is the geopotential, *f* is the Coriolis parameter, *k* is the vertical unit vector, υ is eddy viscosity which can vary, τ is the wind and bottom drag induced shear stress vector, *T* is any one of the model's buoyancy related variables (temperature, salinity, density) and H_T represents the sum of the diabatic source terms acting on *T*. Subscripts show the variables that are kept constant during partial differentiation.

The model employs an Arakawa C-grid distributing the variables such that velocity grid points are located halfway between mass grid points in the *x,y* direction (Arakawa and Lamb, 1977). Thermodynamic variables and variables of motion are treated as layer variables that are constant within layer but change across layer interfaces. However, *p,z* and $\dot{s}\,\partial p/\partial s$ are characterised as level variables defined on

Table 1
Model potential density layers and corresponding salinities

Potential density (σ_θ)	Salinity
13.10	18.02
13.59	18.22
13.85	18.28
14.15	18.41
14.45	18.61
15.05	19.37
15.65	20.19
16.20	20.94
16.45	21.29
16.72	21.65
16.88	21.87
17.05	22.08
17.18	22.25
17.23	22.32

interfaces. A more detailed description of the model, the numerical schemes used and the numerical issues arising from isopycnic modelling can be found elsewhere (see Bleck et al., 1989; Bleck and Smith, 1990; Smith et al., 1990; Bleck et al., 1992; Chassignet and Bleck, 1993; Chassignet et al., 1996; and Bleck, 1998).

3. Model set-up

3.1. Model geometry and density profile

A model resolution of 0.25° longitude × 0.25° $\cos\phi$ latitude was chosen for the horizontal plane and all data files were interpolated to the model grid. Although the full resolution of meso-scale eddy activity is not expected with this relatively coarse horizontal grid, simulation of larger (meso- to large-) scales should be possible. The model includes a surface mixed layer and fourteen potential density layers in the vertical. In order to achieve the sharp vertical stratification found in the basin, average salinity values were specified for each layer. These salinities were calculated by linear interpolation from Altman's data set (1987), which consists of CTD and Nansen bottle measurements made over 70 years. The data comprises monthly averages of temperature and salinity at 22 vertical levels with a resolution of 1° longitude and 0.5° latitude.

Particular effort has been made to choose densities corresponding to the minimum temperature in the CIL (14.45 σ_θ) and its upper and lower bounding layers (14.15 σ_θ and 15.65 σ_θ). The potential densities of suboxic

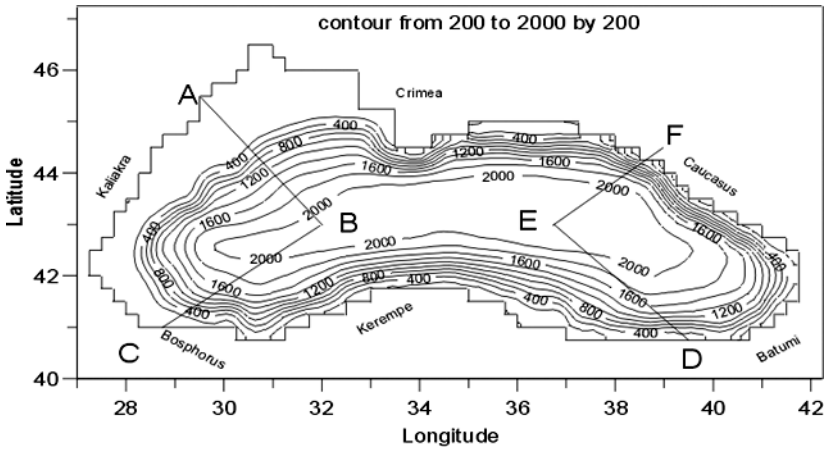

Fig. 1. Model topography (depths are in meters). The straight lines ABC and DEF give the position of the vertical cross sections shown in Fig. 13.

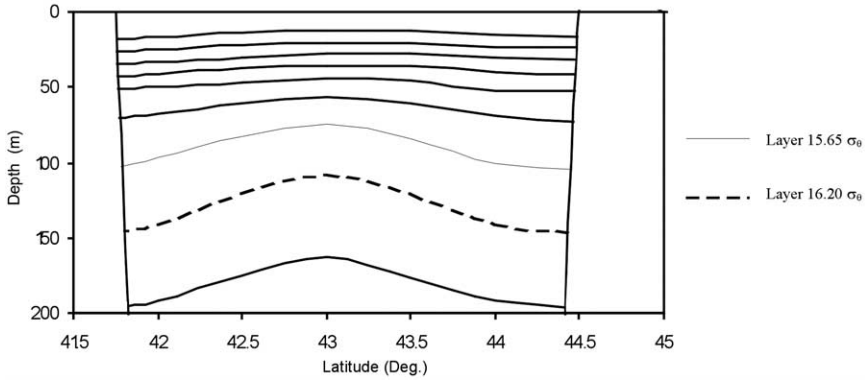

Fig. 2. Layer interfaces in the initialisation along the longitude 34° for the upper 200 m.

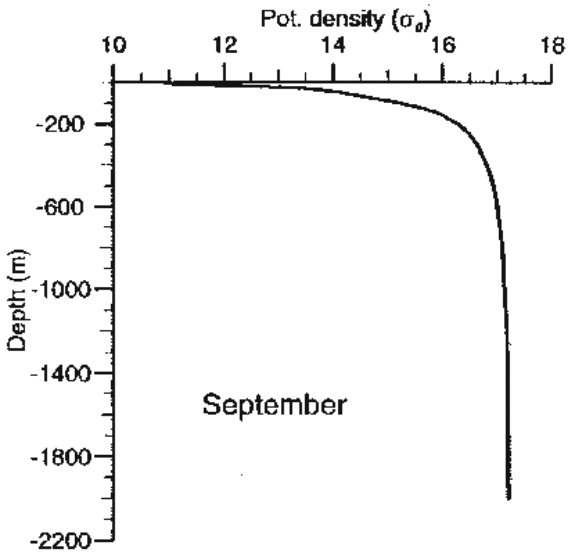

Fig. 3. Basin averaged density profile for September climatology.

layer base (16.72 σ_θ) and bottom mixed layer (17.23 σ_θ) were also specified. The chosen layer densities and corresponding salinity fields are shown in Table 1.

The bottom topography of the basin was interpolated to fit the model grid from the Scripps topography data set. This was subsequently checked with Hydrographic Office charts (Hydrographic Office, 1996). The resultant model bathymetry is shown in Fig. 1. The model was initialised using September climatology with transverse-basin meridional density profiles interpolated from the data set of Altman (1987). In Fig. 2 we show layer interfaces in the initialisation along the longitude 34° for the upper 200 m. The dome-shaped isopycnals are relatively suppressed in this month due to reduced river inflow and summer stratification. A basin-averaged density profile for this month is shown in Fig. 3. Both Kraus-Turner and Gaspar types of mixed layer formulations are available in the model and the latter was chosen with the minimum thickness of the mixed layer specified as 5 m.

3.2. Model forcing and parameterisation

The model is forced by mechanical (wind stress), thermodynamic and relaxation functions. Wind stress data is derived from the Hellermann and Rosenstein (1983) monthly climatologies and interpolated to the model grid. Oguz et al. (1995) report that wind stresses in this set are insufficiently strong but well documented reflecting the main features of the Black Sea winds in space and in time. They also note that Hellermann and Rosenstein fields are 2–3 times weaker compared with measured values from meteorological stations. These comments lead us to increase our Hellermann and Rosenstein data values by a mean factor of 2.5. Fig. 4 shows the wind stress in January and July to represent the change of seasonal wind pattern over

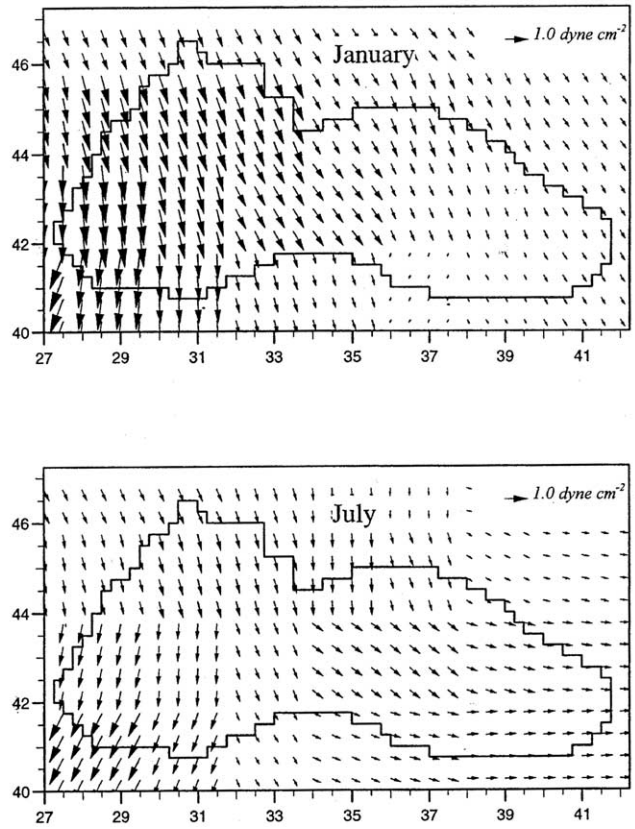

Fig. 4. Model wind stress distribution in January and July.

the basin. Winds are usually strongest in winter. In the western part of the sea, winds from between NE and NW are dominant, while in the west they are usually northwesterly and much lighter. In summer, however, winds are much less strong but in the southeast winds from the west are frequent.

Thermodynamic forcing is based on the calculation of the thermal balance (B):

$$B = R + H + \varepsilon \tag{4}$$

where, R is the balance of incident solar radiation and radiation emitted by the sea surface, ε is the latent heat transfer due to evaporation and H is the sensible heat transfer, which is established by convection when there is a considerable difference between sea surface temperature and air temperature. These components are calculated from precipitation, wind speed, effective air temperature, net radiation at the sea surface and the atmospheric water vapour mixing ratio. Precipitation and wind speed data were compiled and interpolated from Meteorological Office charts (1963). The net radiation at surface is taken as the difference between the incoming short-wave radiation and outgoing long-wave radiation. If t_d is length of day in hours and A_n is noon altitude of the sun in degrees, then the short-wave radiation input in the absence of clouds (Q_{so};

W m^{-2}) and allowing for the average atmospheric loss is (Bunker et al., 1982):

$$Q_{so} = 0.4A_n\, t_d \tag{8}$$

The rate at which the radiant energy arrives at the sea surface (Q'_s; W m^{-2}) after allowing reduction by the ratio of cloud cover (C) is:

$$Q'_s = Q_{so}\,(1 - 0.0012C^3) \tag{9}$$

The amount of short-wave radiation reflected from the sea surface (Q_r):

$$Q_r = 0.15Q'_s - (0.01Q'_s)^2 \tag{10}$$

Finally:

$$Q_s\,(W/m^2) = Q'_s - Q_r = 0.85Q'_s - 10^{-4}\,Q'_s \tag{11}$$

where Q_s is the actual short-wave radiation penetrating into the sea (Bunker et al., 1982). The net rate of heat loss by the sea as long-wave radiation to the atmosphere was taken as the world average value of 50 W m^{-2} (Bunker, 1976). The atmospheric water vapour mixing ratio, q; is found using (Bunker et al., 1982):

$$q = \frac{0.622e}{p - e} \tag{12}$$

where e is the pressure of water vapour in the atmosphere and p is the atmospheric pressure. The values for e and p were interpolated from the charts of the Meteorological Office and Hydrographer of the Navy (1990).

Fig. 5 shows that the model-derived annual basin averaged net heat flux (positive upward from sea to air), ranges from –125 W m^{-2} in summer to 130 W m^{-2} in winter. The data are comparable to those used by Oguz and Malanotte-Rizzoli (1996). The annual mean value implies a loss of 3.5 W m^{-2}, which is balanced by the heat gained from the Bosporus.

Since river runoff is expected to have a crucial effect in determining the physical processes in the basin, runoff input from three major rivers, namely the Danube, Dniester and Dnieper, was added to the precipitation data in the corresponding grid cells on the northwestern shelf. The flow rates used are 219, 48 and 48 km^3 year^{-1} respectively. As for the precipitation data, the seasonal variation of the river flow rates was considered, the extent of this variation was up to ± 30% of the annual mean.

The Bosporus Strait, which is the only source for high saline waters from the Mediterranean was included in the domain as an open boundary where relaxation is applied. Although the relatively coarse resolution of the present model does not give a realistic simulation of the strait, its inclusion helps to reveal the significance of its contribution. Seasonal data for the Bosporus Strait were specified by interpolation from surveys conducted during 1986 (Unluata et al., 1990). Fig. 6 shows the year-averaged profiles of salinity in the region corresponding to the density structure of the model. The salinity values of the bottom layers of the basin are located at much shallower depths in the Bosporus to be able to simulate the Mediterranean influx. The excess of precipitation and river runoff over evaporation amounts to 296 km^3 year^{-1} in the model, and the overall water budget is balanced by the Bosporus flows. In a similar manner, the salt budget of the model basin is closed by the salt influx from the Mediterranean through the Bosporus. Seasonal variation of salt flux varies between 5×10^{-7} kg m^{-2} s^{-1} and 2×10^{-6} kg m^{-2} s^{-1} in the model depending on the seasonal balance of evaporation and precipitation.

In accordance with the suggestions by the Miami group a ratio of 20:1 between the baroclinic and barotropic time steps is chosen and these were set correspondingly at 400 s and 20 s after successively reducing the parameters controlling vertical mixing (e.g. diffusion velocity across mixed layer base was maintained as 1×10^{-5} cm s^{-1}, while the number of time steps between diapycnal mixing calculations was 1080) to attain sharp stratification. Initial oscillations in the sea surface height were not observed. The maximum difference between two successive years is found to be 0.07 cm in November. It was concluded that the model

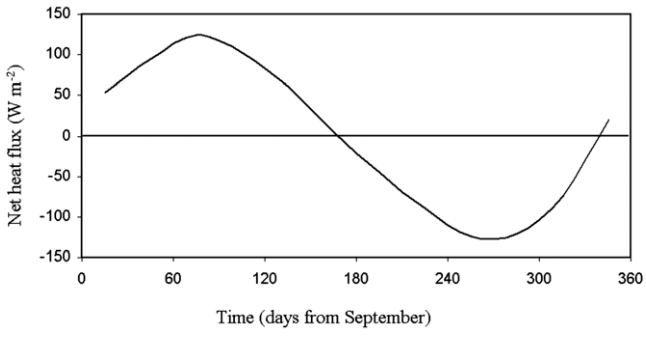

Fig. 5. Basin averaged monthly variation of the net heat flux (positive upward from sea to air).

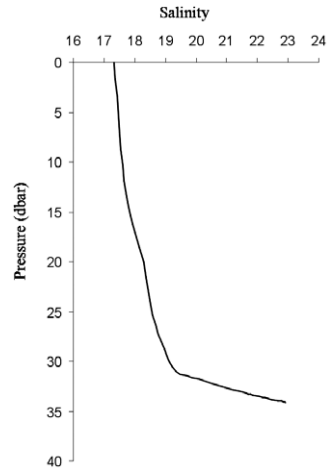

Fig. 6. Year averaged salinity profile of the model at the Bosporus exit region.

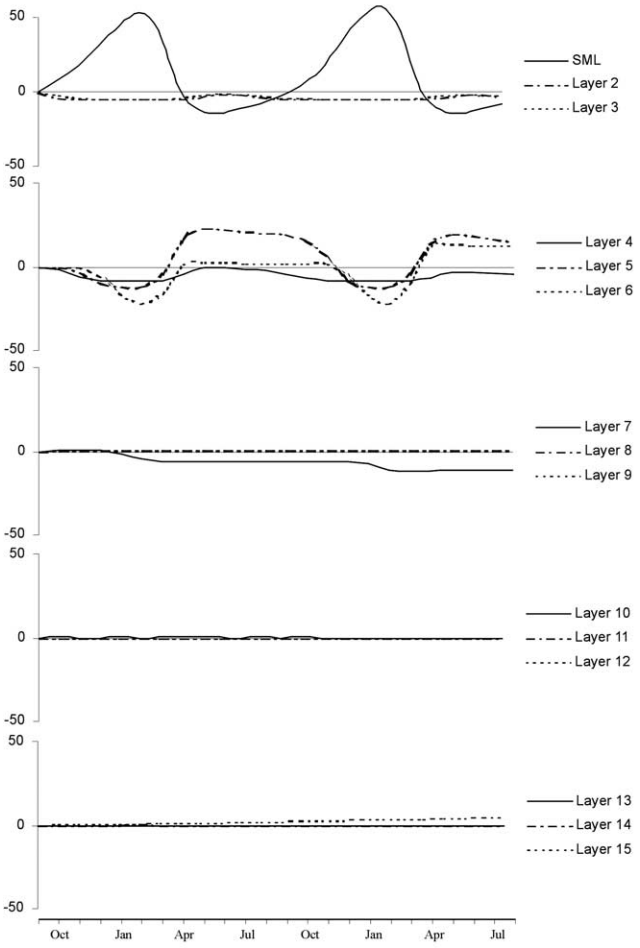

Fig. 7. Basin-averaged layer thickness anomalies in m (differences from the initial state of the total layer volume divided by the basin area) for model layers over two years run (SML represents surface mixed layer, see Table 1 for the rest of layer densities).

was stable and hereafter the results for the second year are presented.

4. Results and discussion

In Fig. 7 we show the time series of the basin-averaged layer thickness anomalies over two years to illustrate the water mass changes in the model layers. The surface mixed layer and the underlying five layers, including the core of CIL (layer 6) appear to have a seasonal signal and interactions with one another. While layer 7 (15.05 σ_θ) has detrained ≈11 m of water by the end of the two year period, the SOL (layer 9) is quite stable, neither gaining or losing water. In contrast, the bottom mixed layer rises by ≈4 m; possibly as a result of the influx of saltier water from the Mediterranean.

Before proceeding with a description of the subsurface dynamics we first present the general characteristics of surface circulation revealed by the present model in order to understand the extent of its influence on the subsurface layers. In Fig. 8 and Fig. 9 we show the circulation in the surface mixed layer in January and July taking these to be representative of winter and summer patterns respectively. The well-known cyclonic rim current flowing along the steep coastline can be clearly observed in winter. It consists of four to six cyclonic gyres extending from west to east between 29° E and 40° E. Although they are not very distinct due to the relatively coarse horizontal resolution of the model, a few anti-cyclonic eddies are apparent. These are confined between the coastline and the rim current and are thought to be formed from the associated effects of bed friction that results in the creation of a shear velocity between the shelf break and the rim current. These eddies are located in the proximity of the Bosporus, on the western side of Crimean peninsula at 44.5° N 32.5° E, along the Caucasian coast at 44° N 38° E and near the Cape Kaliakra at 43.5° N 29° E. The so-called Batumi eddy was not visible in our January model results in the easternmost part of the basin. The existence of the various eddy structures is reported by a number of authors using various sets of

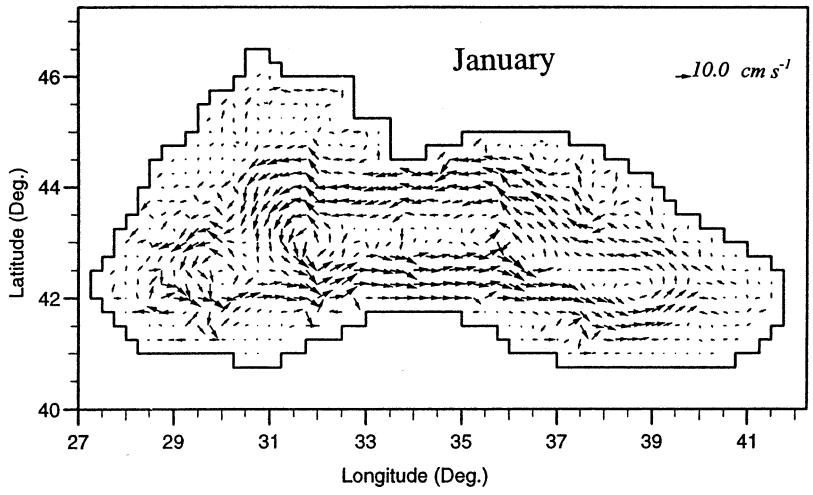

Fig. 8. January circulation in the surface mixed layer (maximum current speed was set to 10 cm s^{-1} for clear presentation).

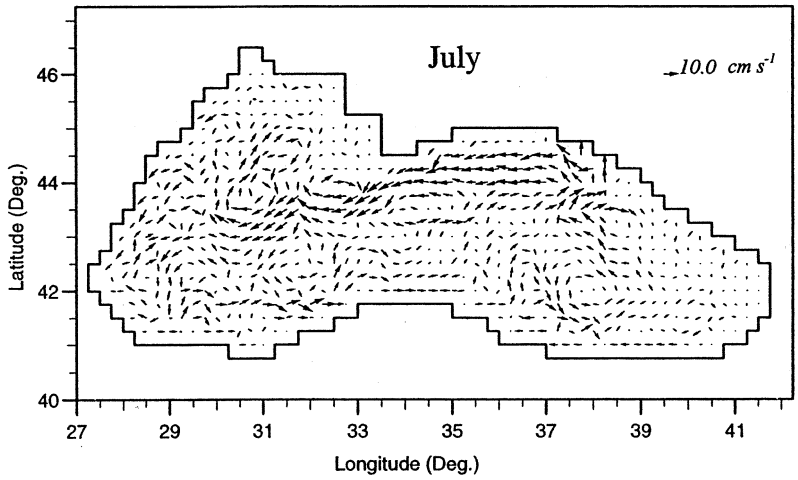

Fig. 9. July circulation in the surface mixed layer (maximum current speed was set to 10 cm s^{-1} for clear presentation).

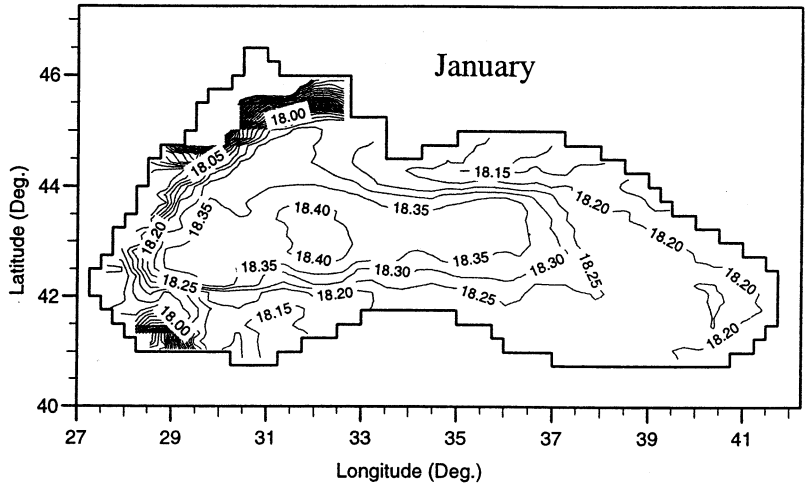

Fig. 10. January salinity distribution in the surface mixed layer.

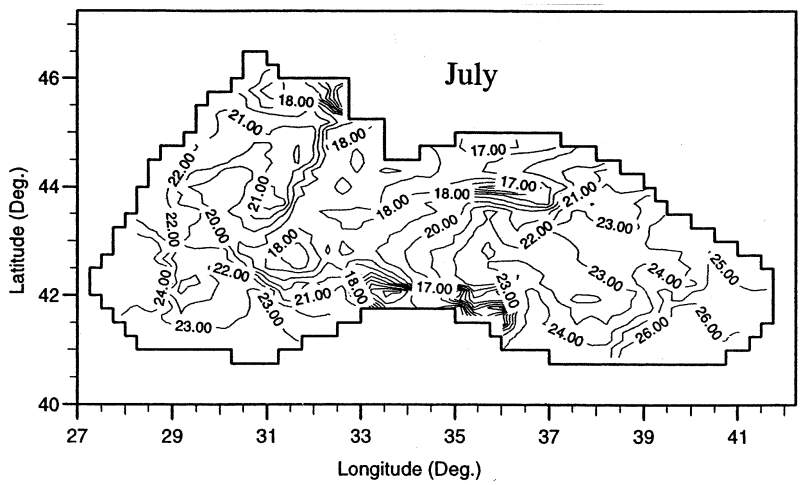

Fig. 11. July temperature (ºC) distribution in the surface mixed layer.

hydrographic observations (see Trukchev et al., 1985; Titov, 1992; Oguz et al., 1993; Oguz et al., 1994; Ozsoy and Unluata, 1997). The distribution of surface layer salinity is easily correlated with the circulation pattern in winter (see Fig. 10). Highly saline waters are trapped in the rim current and are surrounded by fresher waters resulting from river runoff or heavy precipitation. Furthermore, the salinity contrast between interior and coastal waters is sharper in the

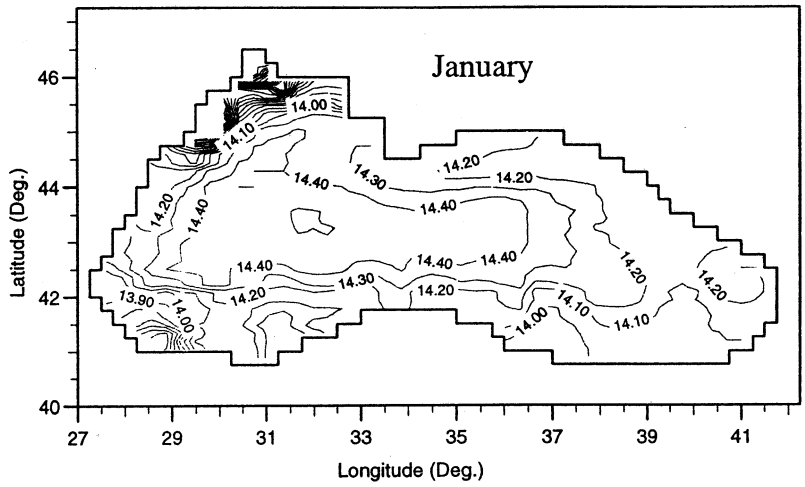

Fig. 12. January density (kg m^{-3}) distribution in the surface mixed layer.

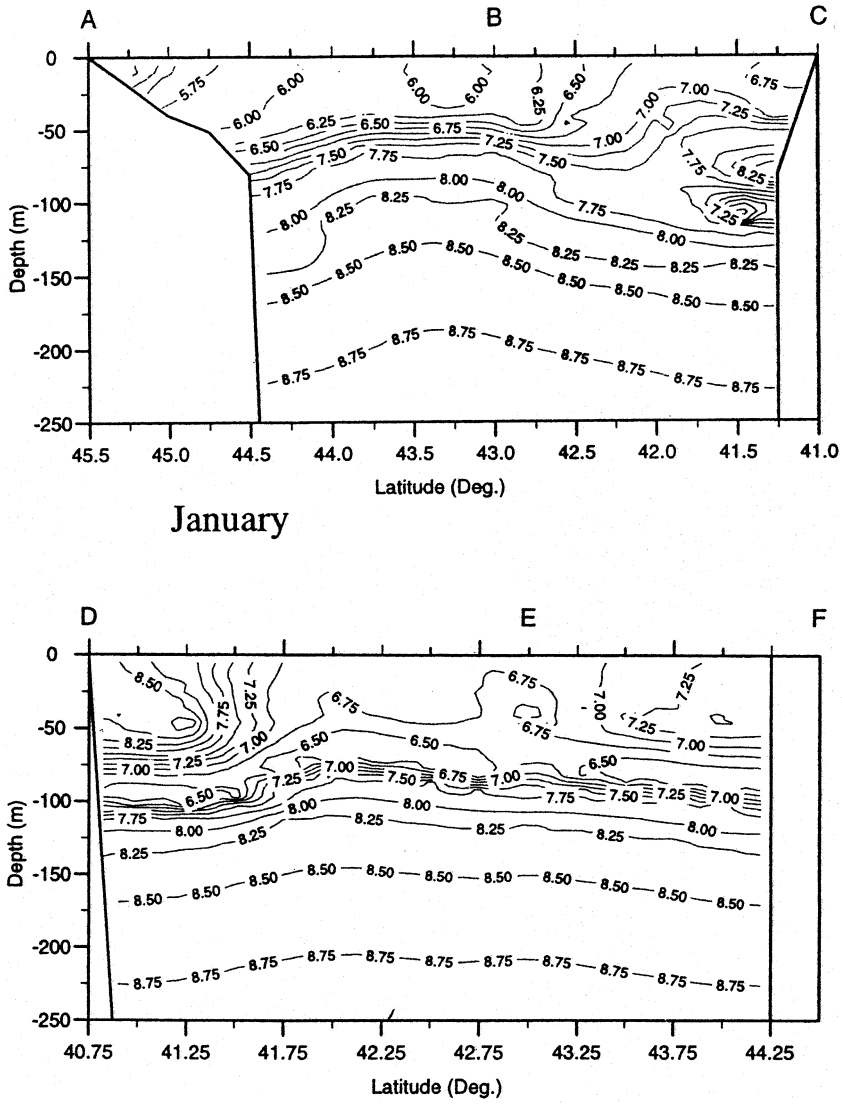

Fig. 13. Vertical temperature (ºC) distribution in the upper 250 m in January along sections ABC and DEF.

western part of the basin than in the eastern part due to inputs from the Danube, Dniester and Dnieper in the NW shelf. Very low salinity values, less than 17, are found in this shallow region. Low salinity waters, starting from the western side of the Crimean Peninsula, follows the coastal topography and elongates until the Bosporus region with a crescent-like shape. The typical salinity of this belt is approximately 18.05. In the eastern part of the sea, lowest salinity values are encountered around the northern Caucasian coast as low as 18.10 at 44° N. The salinity increases towards the interior of the basin. The highest salinities, around 18.40, are observed in the centre of the western cyclonic gyre.

The rim current changes its path with its eddies shifting their centres in summer (see Fig. 9). The number of eddies along the Anatolian coast substantially increases so that the rim current can be hardly distinguished in the southern and eastern Black Sea. For the north and west regions, on the other hand, it is not difficult to track the rim current as it persists along 44° N, although enlarging anti-cyclonic eddies push it towards the interior part of the basin. It is worth noting that displacement of the rim current from its route in summer brings about the formation of a few cyclonic eddies in the eastern part outside the ring of the rim current. Corresponding sea surface temperatures (see Fig. 11) in July vary from 17.0 °C to 26.0 °C throughout the basin and in general there is an increase from north to south. However, water patches as cold as 17 °C are observed along the Anatolian coast. It is likely that the colder patches are linked to water upwelling along the coast and are a feature of the anti-cyclonic eddies that occur here. Comparable, persistent upwelling events have been reported near Cape Kaliakra in the west and along the Anatolian coast. The latter events are found to recur almost every summer even though the wind patterns do not favour their formation (see Sur et al. (1994), and Ozsoy and Unluata (1997)).

The January distribution of density in the surface mixed layer allows us to infer that the wind system over the basin and the topography are not the sole factors controlling the upper layer cyclonic boundary current. As illustrated in Fig. 12, the density distribution shows similarities with the salinity distribution, in that density of the water masses

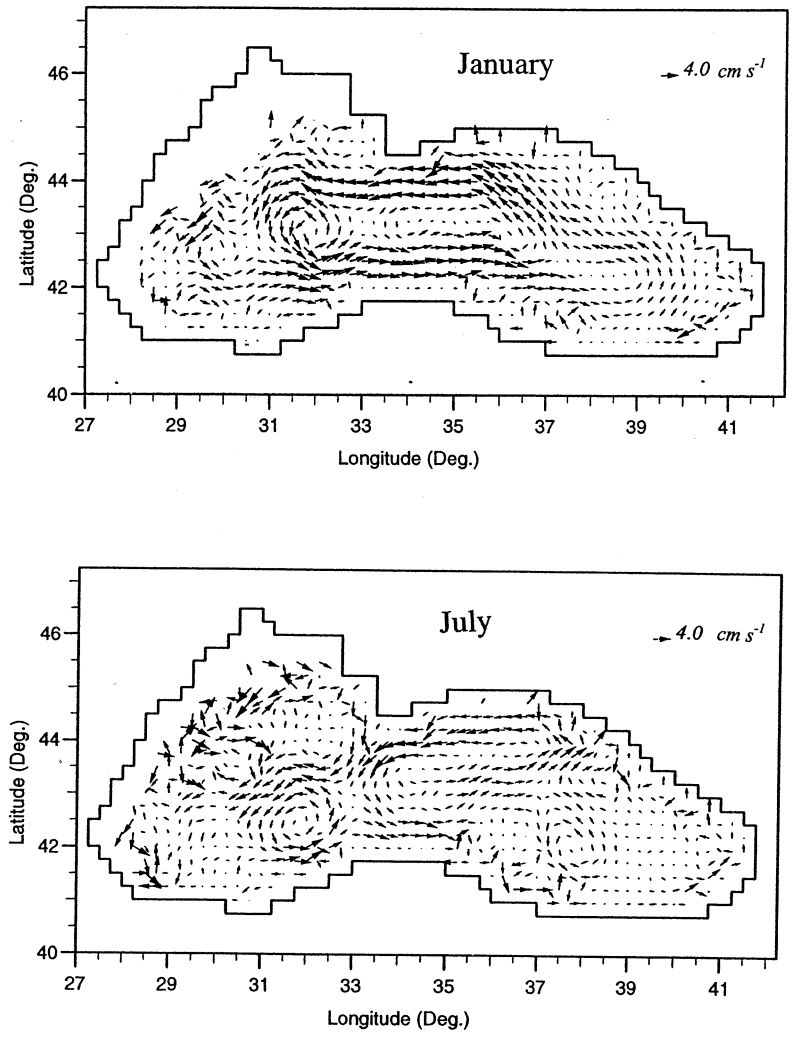

Fig. 14. Circulation on the CIL (maximum current speed was set to 4 cm s^{-1} for clear presentation).

increases towards the inner part of the basin giving rise to dome-shaped isopycnals and suggesting that salinity is the main control on baroclinic flow. The lowest densities over the entire year are encountered in the far northwestern shelf region of the sea at 45° N 31° E. The highest density, on the other hand, is observed (14.50 kg m^{-3}) in the centre of the western gyre of the rim current.

Fig. 13 depicts the vertical temperature distribution in January for the upper 250 m in a vertical section through the points ABC and DEF shown on Fig. 1. It is seen that river runoff from the NW shelf and water exiting from the Bosporus depress the isopycnals along the shelf and force the high density waters towards the basin interior, intensifying the pressure gradients driving the cyclonic flow. It is also noticeable from this figure that the 8 °C isotherm characterising the Cold intermediate layer follows the dome-shaped depression of the isopycnals.

Adjacent subsurface layers have similar features of circulation patterns as the surface layer, while showing less complexity. Fig. 14 illustrates the circulation on the layer with density 14.45 σ_θ, which has been identified as the density of the CIL core following the HydroBlack '91 surveys (Oguz et al., 1994). In January the cyclonic rim current is again found to be the dominant feature and in addition, fewer secondary gyres are apparent. In contrast by July the rim current has become less recognisable and the circulation appears to comprise of independent cyclonic gyres in the interior of the basin while anti-cyclonic eddies are found along the coastal regions. Fig. 15 shows the seasonal topography of the 8 °C isotherm at the base of the CIL. The bottom boundary of the CIL, which is found between 70 to 130 m below the sea surface throughout the year, is not subject to major movement suggesting that thickness of this layer is mainly dependent upon changes in the dynamics of the upper layers. The seasonal response to the upper layer dynamics is obvious in the July topography of the base of the CIL, which is depressed in the south-western part of the basin as a result of the anti-cyclonic eddy formed in that vicinity.

Although weaker, the main features of circulation in the layer 16.20 σ_θ, which defines the lower boundary of the suboxic zone, are almost identical to those in the layer discussed previously, as shown in Fig. 16. The major water movements in this layer comprise the rim current, which contains four main cyclonic gyres, and several anti-cyclonic eddies that are confined between the coast and the rim current. The latter are located near Crimean Peninsula, along the Caucasian coast, near Cape Kaliakra and near Batumi in January. The July circulation suggests that following shifts in the centres of the anti-cyclonic gyres and growth in the size of the anti-cyclonic eddies, the rim current cannot be easily discerned in summer. Comparison of Figs 17 and 18 suggests similarities between the 16.2 σ_θ potential density surface found in the HydroBlack '91 survey (Oguz et al., 1994) and the comparable October topography obtained from the present model (note that the

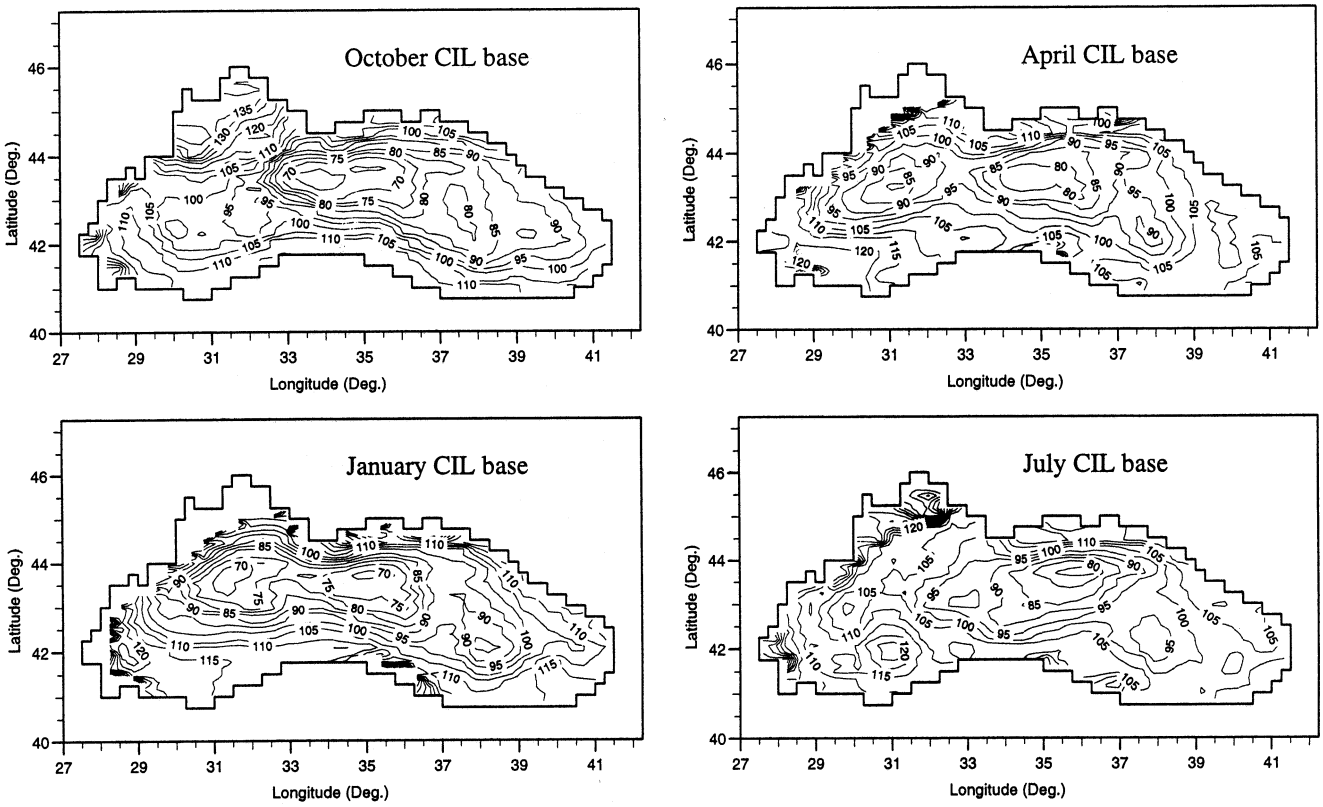

Fig. 15. Seasonal topography of the 8 ºC isotherm at the base of the CIL.

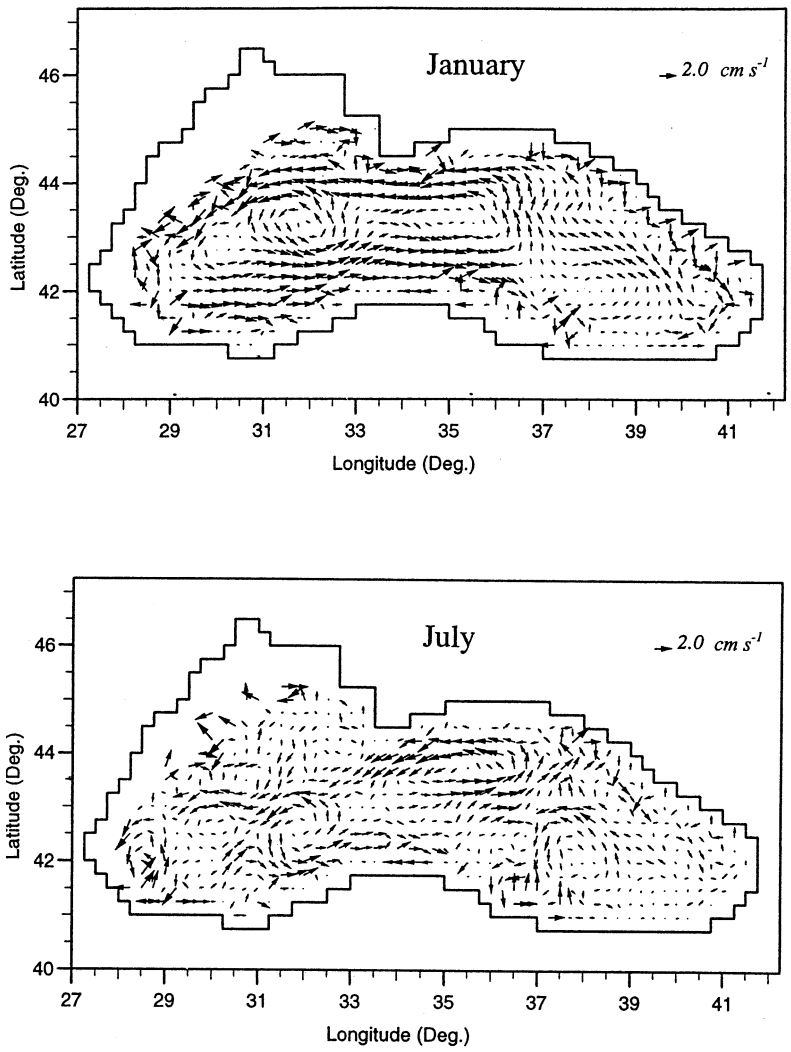

Fig. 16. Circulation on the 16.2 σ_θ potential density surface (lower interface of the SOL) (maximum current speed was set to 2 cm s^{-1} for clear presentation).

layers are indexed with their upper interfaces in the model). The density surface in both figures changes from ≈110 m below the sea surface in the central region to ≈180 m along the periphery of the basin confirming the notion that it is shaped like a dome. However, the meandering of the isopycnals cannot be fully determined, as the coarsely resolved coastline of the model does not allow a more precise representation to be presented. In addition, monthly averaged forcing which overrides short-term atmospheric dynamics could be another factor for the poor resolution. Fig. 19 shows the depth of the 16.2 σ_θ potential density surface in January, April and July. In a manner similar to the base of the CIL, the depth of the SOL interface does not exhibit large seasonal variations. The SOL is located between 110 m and 170 m below the surface in the central and coastal regions of the basin respectively throughout the year and follows the dome-shaped isopycnal surfaces. Nevertheless increasing eddy activity is linked to a shift in the location of the deeper and shallower parts of the SOL boundary during the spring and summer months.

Table 2 shows the maximum model velocities observed in the surface layers. It is interesting to note that velocities in the layers adjacent to the surface mixed layer are always higher than those found at the surface, and that higher velocities are seen in the upper layers during the summer and spring. Below this, there is a gradual decrease in velocity with depth towards the intermediate layers. The magnitudes of the velocities shown are in agreement with reported ADCP measurements (Oguz and Besiktepe, 1999) where velocities of up to 1 m s^{-1} are found in the upper 100 m of the water.

Results obtained from the present model suggest the existence of a rim counter-current in the deeper layers throughout the year. Fig. 20 shows the circulation in layers 16.72 σ_θ, 17.06 σ_θ and 17.23 σ_θ in January, July and October respectively. In particular, the 16.72 σ_θ layer shows the first deviations from those in the upper layers and represent the transition between upper and lower water motions. Although the cyclonic rim current can still be detected in the interior of the basin, it is encircled by an opposing current

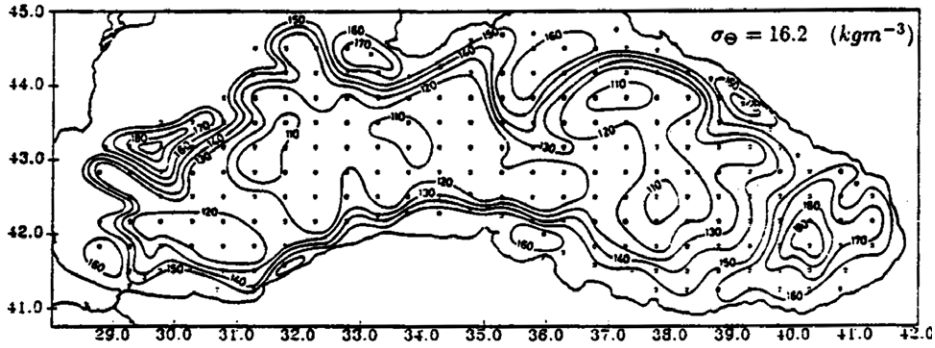

Fig. 17. The topography of 16.2 σ_θ potential density surface, defining lower boundary of the SOL in the HydroBlack'91 survey (after Oguz et al., 1994)

that flows along the coastal slope. The counter current has strengthened by the 17.06 σ_θ layer and in addition no major seasonal changes in circulation can be detected, indicating that the strong stratification of the Black Sea prevents the effects of seasonal forcing from reaching to the lower layers. A clearer representation of the anti-cyclonic rim current, found in the bottom layers of the Black Sea, is shown in the potential density layer corresponding to 17.23 σ_θ, which is known as the upper interface of the bottom mixed layer. The anti-cyclonic deep rim current in this layer comprises four gyres.

The influx of saltier water from the Bosporus and fresh water runoff from the NW shelf region appear to be the underlying factors driving this deep anti-cyclonic boundary current system. These fluxes generate density gradients, which, together with the Coriolis force, encourage an anti-cyclonic current regime in the deep layers of the basin. In a previous study, Korotaev (1997) uses a simple model to predict another cyclonic current at bottom depths below the anticylonic counter current. In contrast with this author's work, the results obtained from the present model do not show this large-scale feature and it is possible that the formation of the additional feature is suppressed by effects generated by the more realistic topography and forcing used in the present work.

5. Conclusions

An ocean circulation model using isopycnic coordinates has been used to examine the seasonal variation of subsurface water dynamics in relation to the surface layer. Par ticular attention has been paid to the waters of the CIL, the SOL and the deep layer circulation of the Black Sea. It is shown that the interfacial region between the base of the CIL and the SOL is unaffected by seasonal change. However, the position of the deeper and shallower regions varies with the seasonal upper layer dynamics of the basin. The vertical movement of the upper interface of the CIL, significantly determines the thickness of this layer.

The model results suggest that deep layer circulation in the Black Sea is characterised by the reversal of the cyclonic rim current, which results from the density gradients created by water influx from the Mediterranean and freshwater runoff from the north-western shelf region. It is also notable that the present model produces strong gyres in the western part of the basin, in particular in the surface and subsurface layers. Once again the strong density gradients and wind fields found in the west account for this.

Neither the resolution of the model presented here, nor the available data, are sufficient to give precise details of finer aspects of circulation in the Black Sea basin (e.g.,

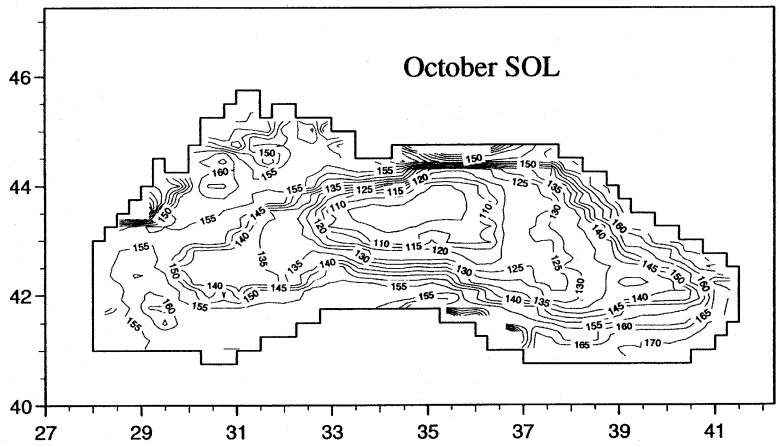

Fig. 18. The model topography of 16.2 σ_θ potential density surface in October.

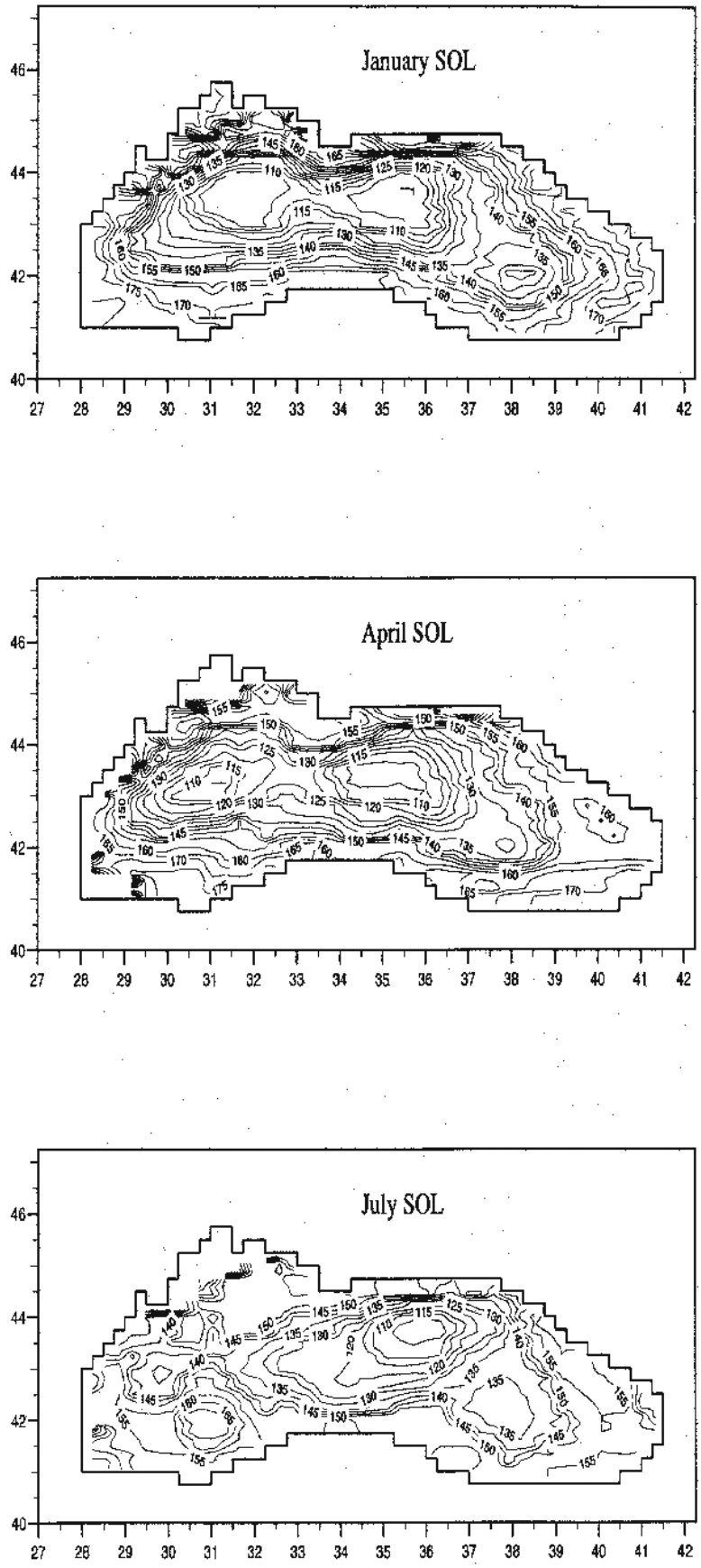

Fig. 19. The model topography of 16.2 σ_θ potential density surface in January, April and July.

Table 2
Maximum model velocities observed in the surface and intermediate layers (0 cm s^{-1} velocities in the subsurface layers in October and January indicate deepening mixed layer (entrainment)).

Potential density layer (σ_θ)	Maximum model velocities (cm s^{-1})			
	October	January	April	July
Surface mixed layer	39.89	33.67	48.86	49.64
13.10	0	0	97.29	71.47
13.59	55.32	0	95.01	62.57
13.85	32.92	0	45.41	62.33
14.15	33.57	0	58.69	58.48
14.45	22.54	78.48	20.67	23.46
15.05	30.05	22.88	21.46	25.71
15.65	28.48	29.45	36.29	25.05

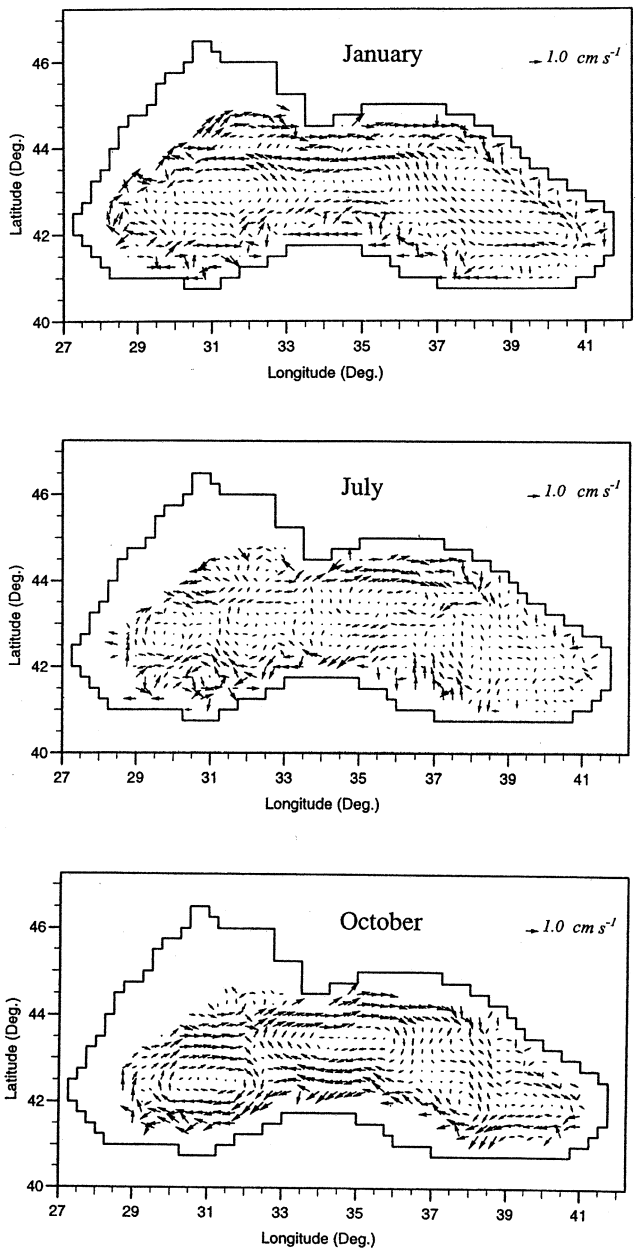

Fig. 20. Circulation in potential density layers 16.72 σ_θ, 17.06 σ_θ and 17.23 σ_θ (maximum current speed is set to 1 cm s^{-1} for clear presentation).

meandering currents, meso-scale eddy activity and Rossby waves). However, the relative success of the present approach suggests that further development of isopynic models with higher resolution in both vertical and horizontal coordinates together with the acquisition of improved fine resolution climatologies, will lead to better understanding the dynamics of the basin. In particular, the exaggerated influx of saltier water through the Bosporus can be avoided and the rise of the bottom mixed layer interface could be moderated in a long-term integration of the model. Finally, a more accurate portrayal of changes in the current regime in the subsurface layers and the extent to which the seasonal atmospheric forcing signals penetrate into intermediate and deeper layers against the strong density stratification are of fundamental importance to the improved understanding of the biogeochemistry of the basin.

Acknowledgements

The authors would like to express their gratitude to Dr Linda Smith and Dr Reiner Bleck of Rosenstial School of Marine and Atmospheric Sciences, University of Miami and Dr Vassil Roussenov of Liverpool University for their constructive advice during the setting up of the model. In addition, we would like to thank to Dr Temel Oguz of Erdemli Institute of Marine Sciences for providing Altman's data set.

References

Altman, E.N., Gertman, I.F., Golubeva, Z.A., 1987. Climatological Fields of Salinity and Temperature in the Black Sea. Sevastopol Branch. State Oceanography Institute, Sevastopol, Ukraine, pp. 109–109.

Arakawa, A., Lamb, V.R., 1977. Computational design of the basic processes of the UCLA General Circulation Model. Methods Comp. Phys. 17, 174–265.

Baştürk, O., Tuğrul, S., Konovalov, S., Salihoğlu, I., 1997. Variations in the vertical structure of water chemistry within the three hydrodynamically different regions of the Black Sea. In: Özsoy, E., Mikaelyan, A (Eds.), Sensitivity to Change: Black Sea, Baltic Sea and North Sea. Kluwer Academic Publishers, pp. 183–196.

Bleck, R., 1978. Finite Difference Equations in Generalized Vertical Coordinates, Part 1: Total Energy Conservation. Contrib. Atmos. Phys. 51, 360–372.

Bleck, R., Hanson, H.P., Hu, D., Kraus, E.B., 1989. Mixed layer/thermocline interaction in a three-dimensional isopycnal model. J. Phys. Oceanogr. 19, 1417–1439.

Bleck, R., Smith, L., 1990. A Wind-Driven Isopycnic Coordinate Model of the North and Equatorial Atlantic Ocean 1: Model Development and Supporting Experiments. J. Geopyhs. Res. 95, 3273–3285.

Bleck, R., Rooth, C., Hu, D., Smith, L.T., 1992. Salinity-driven Thermocline Transients in a Wind- and Thermohaline-forced Isopycnic Coordinate Model of the North Atlantic. J. Phys. Oceanogr. 22, 1486–1505.

Bleck, R., 1998. Ocean modeling in isopycnic coordinates. In: Chassignet, E.P., Verron, J. (Eds.), Ocean Modeling and Parameterization. Kluwer Academic Publishers, pp. 423–448.

Bulgakov, S.N., Kushnir, V.M., 1996. Vertical structure of the current field in the Northern Black Sea. Oceanol. Acta 19 (5), 513–522.

Bunker, A.F., 1976. Computation of surface energy flux and annual air-sea interaction cycles of the North Atlantic Ocean. Mon. Weather Rev. 104, 1122–1140.

Bunker, A.F., Charnok, H., Goldsmith, R.A., 1982. A note on the heat balance of Mediterranean and Red Seas. J. Mar. Res. 40, 73–84.

Chassignet, E.P., Smith, L.T., Bleck, R., Bryan, F., 1996. A Model Comparison: Numerical Simulations of the North and Equatorial Atlantic Oceanic Circulation in Depth and Isopynic Coordinates. J. Phys Oceanogr. 26, 1849–1867.

Chassignet, E.P., Bleck, R., 1993. The influence of layer outcropping on the separation of boundary currents. Part I: The wind-driven experiments. J. Phys. Oceanogr. 23, 1485–1507.

Eremeev, V.N., Kushnir, V.M., 1996. The Layered Structure of Currents and Vertical Exchange in the Black Sea. Oceanology 36, 9–15.

Filippov, D.M., 1965. The Cold Intermediate Layer in the Black Sea. Oceanology 5, 47–52.

Ginsburg, A.I., 1995. Horizontal water exchange in the subsurface layer of the Black Sea. Earth Observ. Remote Sens. 12, 236–248.

Hellermann, S., Rosenstein, M., 1983. Normal monthly wind stress over the World Ocean with error estimates. J. Phys. Oceanogr. 13, 1093–1104.

Hydrographer of the Navy, 1990. Black Sea Pilot, 12th edition. HMSO, Somerset, pp. 231–231.

Hydrographic Office, 1996. The Black Sea including the Marmara Denizi and the Sea of Azov. Chart No 2214, Somerset, UK.

Ivanov, L.I., Besiktepe, S., Ozsoy, E., 1997. The Black Sea Cold Intermediate Layer. In: Özsoy, E., Mikaelyan, A (Eds.), Sensitivity to change: Black Sea, Blatic Sea and North Sea. Kluwer Academic Publishers, pp. 264–523.

Konovalov, S., Tuğrul, S., Baştürk, O., Salihoğlu, I., 1997. Spatial isopycnal analysis of the main pycnocline chemistry of the Black Sea: seasonal and interannual variations. In: Özsoy, E., Mikaelyan, A (Eds.), Sensitivity to Change: Black Sea, Baltic Sea and North Sea. Kluwer Academic Publishers, pp. 197–210.

Korotaev, G.K., 1997. Circulation in semi-enclosed seas induced by buoyancy flux through a strait. In: Özsoy, E., Mikaelyan, A (Eds.), Sensitivity to change: Black Sea, Blatic Sea and North Sea. Kluwer Academic Publishers, pp. 197–210.

Meteorological Office, 1963. Weather in the Black Sea. HMSO, London, pp. 291–291.

Murray, J.W., Top, Z., Ozsoy, E., 1991. Hydrographic properties and ventilation in the Black Sea. Deep-Sea Res. 38, S663–S689.

Oguz, T., Latif, M.A., Sur, H.I., Ozsoy, E., Unluata, U., 1991. On the dynamics of the southern Blaxk Sea. In: Izdar, E., Murray, W (Eds.), Black Sea Oceanography. Kluwer Academic Publishers, pp. 43–64.

Oguz, T., Latun, V.S., Latif, M.A., Vladimirov, V.V., Sur, H.I., Markov, A.A., Ozsoy, E., Kotovshchikov, B.B., Eremeev, E.E., Unluata, U., 1993. Circulation in the surface and intermediate layers of the Black Sea. Deep-Sea Res. I 40 (8), 1597–1612.

Oguz, T., Aubrey, D.G., Latun, V.S., Demirov, E., Koveshnikov, L., Sur, H.I., Diaconu, V., Besiktepe, S., Duman, M., Limeburner, R., Eremeev, V., 1994. Mesoscale circulation and thermohaline structure of the Black Sea observed during HydroBlack '91. Deep-Sea Res. I 44 (4), 603–628.

Oguz, T., Malanotte-Rizzoli, P., Aubrey, D., 1995. Wind and thermohaline circulation of the Black Sea driven by yearly mean climatological forcing. J. Geophys. Res. 100 (C4), 6845–6863.

Oguz, T., Malanotte-Rizzoli, P., 1996. Seasonal variability of wind and thermohaline-driven circulation in the Black Sea: Modeling studies. J. Geophys. Res. 101 (C7), 16551–16569.

Oguz, T., Besiktepe, S., 1999. Observations on the Rim current structure, CIW formation and transport in the western Black Sea. Deep-Sea Res. I 46, 1733–1754.

Ovchinnikov, I.M., Popov, Y.I., 1987. Evolution of the Cold Intermediate Layer in the Black Sea. Oceanology 27 (5), 555–560.

Ozsoy, E., Unluata, U., 1997. Oceanography of the Black Sea: a review of some recent results. Earth Sci. Rev. 42, 231–272.

Saydam, C., Tuğrul, S., Baştürk, O., Oğuz, T., 1993. Identification of the oxic/anoxic interface by isopycnal surfaces in the Black Sea. Deep-Sea Res. I 40, 1405–1412.

Smith, L.T., Boudra, D.B., Bleck, R., 1990. A Wind-driven Isopycnic Coordinate Model of the North and Equatorial Atlantic Ocean 2: The Atlantic Basin Experiments. J. Geophys. Res. 95, 13105–13128.

Sorokin, Y.I., 1983. The Black Sea. In: Ketchum, B.H (Ed.), Ecosystems of the World: Estuaries and Enclosed Seas. Elsevier, Amsterdam, pp. 253–292.

Sur, H.I., Ozsoy, E., Unluata, U., 1994. Boundary current instabilities, upwelling, shelf mixing and eutrophication processes in the Black Sea. Prog. Oceanogr. 33, 249–302.

Titov, V.B., 1992. On the role of eddies in the formation of the current regime on the Black Sea shelf and in the ecology of the coastal zone. Oceanology 32 (1), 24–30.

Tolmazin, D., 1985. Changing coastal oceanography of the Black Sea, I. Northwestern shelf. Prog. Oceanogr. 15, 217–276.

Trukhchev, D.I., Stanev, Y.V., Balashov, G.D., Miloshev, G.D., Rusenov, V.M., 1985. Some Unique Features of the Mesoscale Structure of Hydrological Fields in the Western Part of the Black Sea. Oceanology 25 (4), 443–446.

Tuğrul, S., Baştürk, O., Saydam, C., Yılmaz, A., 1992. Changes in the hydrochemistry of the Black Sea inferred from water density profiles. Nature 359, 137–139.

Unluata, U., Oguz, T., Latif, M.A., Ozsoy, E., 1990. On the Physical Oceanography of the Turkish Straits. In: Pratt, L.J. (Ed.), The Physical Oceanography of Sea Straits. Kluwer Academic Publishers, Netherlands, pp. 25–60.